Optical Fiber Technology 70 (2022) 102857

Contents lists available at ScienceDirect

Optical Fiber Technology

journal homepage: www.elsevier.com/locate/yofte

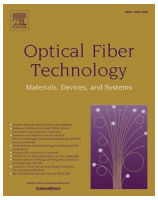

Regular Articles

Thermo-optical numerical modal analysis of multicore fibers for high power lasers and amplifiers

Lorenzo Rosa [a,b], Seyyedhossein Mckee [c], Federica Poli [c], Annamaria Cucinotta [c], Luca Vincetti [a,*]

[a] Department of Engineering "Enzo Ferrari", University of Modena and Reggio Emilia, Modena 41125, Italy
[b] Applied Plasmonics Lab, CMP, Swinburne University of Technology, Hawthorn, VIC 3122, Australia
[c] Department of Engineering and Architecture, University of Parma, Parma 43124, Italy

ARTICLE INFO

Keywords:
Optical fibers
Multicore fibers
Fiber lasers and amplifiers
Coupled mode theory
Finite-element method
Thermal effects

ABSTRACT

Lasers for modern industrial and research applications are required to provide a high average beam power and at the same time be reliable, efficient, and compact. Rare-earth doped single-mode fiber lasers are the most promising solution. Large mode area fibers are effectively used to reduce nonlinear effects and scaling up the beam power which is now bounded by thermal effects. A new cutting-edge approach to the issue involves the use of Multi-Core Fibers (MCFs), coherently combining several lower power beams into a higher power one, and thus pushing the threshold of nonlinearities and transverse mode instabilities to higher power. The amplification process involves heat generation in the doped cores due to quantum defect, which propagates radially and creates a temperature gradient across the fiber cross-section. Even though the cores are optically uncoupled, the refractive index gradient due to thermo-optical effects could cause cross-talk and core mode coupling. In this work, we numerically analyze the performances of 9-core MCFs for high power fiber lasers by taking into account the coupling and bending effects due to the heat load generated by the quantum defect between pump and laser radiation. MCFs show very low sensitivity to heat load and bending, with effectively single-mode behaviour up to 15 μm core diameter (effective area 181 μm^2) and down to 35 μm pitch.

1. Introduction

Fiber-based lasers and amplifiers have come to be increasingly at the center of attention due to their unique characteristics of high average power along with high efficiency, compactness, and reliability, leading to a rapid expansion in industrial applications [1,2]. Over the last 20 years, the output average power of fiber laser and amplifier systems (both continuous wave and pulsed) has experienced an exponential growth [3]. In the classical approaches the nonlinear effects caused by high intensity levels are mitigated by trying to increase as much as possible the fiber mode area. However, large mode area fibers (LMAFs) are affected by the damaging feature of thermal effects, which limit the power scaling of rare-earth doped single-mode fiber lasers. In addition, when LMAFs are bent or coiled, the fundamental mode is squeezed towards the outside of the bend and its effective area is dramatically reduced, scaling back the advantages of LMAFs.

Multi-core fibers (MCFs) are optical fibers having multiple cores inside the cladding region and can be used to improve the threshold limit of nonlinearities and transverse mode instability [4–9], by combining several lower power beams coherently to obtain a single higher power one. However, the heat load on the doped cores, originated by the quantum defect in the amplification process, generates a heat flux flowing from a core through the adjacent ones. This creates a temperature gradient, which induces a refractive index variation following the temperature profile, giving the possibility for thermal cross-talk and leading to possible unwanted coupling between cores, which could affect beam generation and amplification by making specific modes belonging to different cores become degenerate, forming supermodes [10].

In this work, the modal properties, in terms of core coupling, effective area, and effective monomodality, of Yb^{3+}-doped MCFs for high power applications are thoroughly numerically investigated by combining thermal and optical models, in a novel evolution of earlier more basic approaches on multi-core fibers [11]. The finite-element method (FEM) is employed to implement and integrate such models, as it has been successfully done to study mode power evolution and gain

* Corresponding author.

https://doi.org/10.1016/j.yofte.2022.102857
Received 21 November 2021; Received in revised form 14 February 2022; Accepted 26 February 2022
Available online 14 March 2022

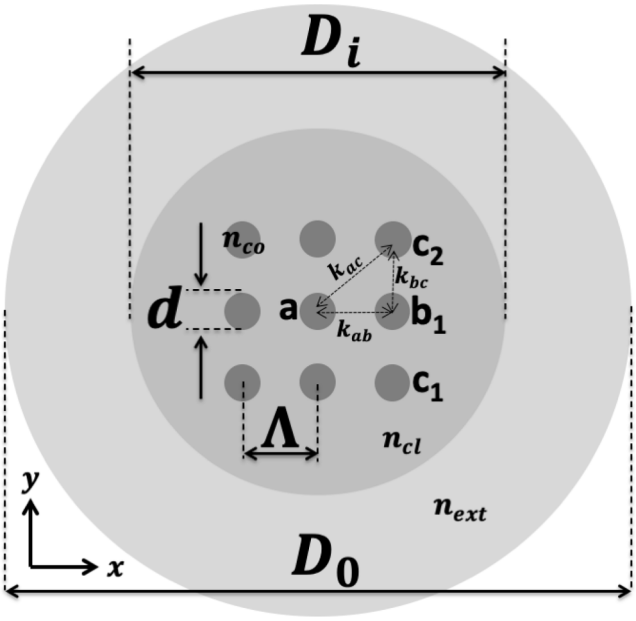

Fig. 1. Geometry of the 9-core MCF and nomenclature of the doped cores by family (a, b, and c) for the analysis.

competition [12]. MCFs show remarkable robustness to heat load and bending; thus, they can properly and effectively work both in rod and coiled configurations. According to the results here showed, a 9-core MCF with cores having numerical aperture (NA) of 0.06 shows effectively single-mode behaviour up to 15 μm core diameter (effective area 181 μm^2 per core) and core decoupling with pitch as low as 35 μm, resulting in a total occupied area of 85×85 μm^2.

2. Numerical model

In the study we consider a MCF with nine Yb^{3+} doped silica cores of diameter d between 12 and 19 μm, placed in an equally-spaced 3x3 square grid inside a silica cladding. The geometry is shown in Fig. 1, where the core refractive index is $n_{co} = 1.45$ and the inner-cladding refractive index is $n_{cl} = 1.4487$, for a numerical aperture NA of 0.06, while the center-to-center core distance or pitch Λ is variable between 25 and 55 μm. The silica inner cladding has diameter $D_i = 420$ μm and the outer cladding $D_o = 600$ μm. The refractive index is lowered to $n_{ext} = 1.37$ in the outer cladding to increase pump field confinement. All these parameters are compatible with today's state of the art in MCFs [5] and while core diameters larger than 20 μm are possible, they entail a dramatic reduction of the numerical aperture in order to keep the index contrast within practical limits [9], so they were not considered here. The fiber was simulated at the typical wavelength of $\lambda = 1032$ nm for the activity of the Yb^{3+} doping ions, which for amplification purposes usually have concentrations around $5{\cdot}10^{25}$ ions/m^3 [9]. We apply to each core an equal heat load q, as a source for the thermal simulation that outputs the temperature profile from which the refractive index profile is calculated. In the amplification process, this heat load is given by the quantum defect due to the wavelength difference between pump and signal photons [13]. Mode electric field distributions of a cold MCF with $\Lambda = 55$ μm and $d = 15$ μm are shown in Fig. 2. The V-number of the single core at $\lambda = 1032$ nm is 2.80. Each core of the MCF supports the Fundamental Mode (FM) LP_{01} and the Higher-Order Modes (HOMs) LP^t_{11} and LP^n_{11}, identified by having the zero intensity line tangential and normal to the reference plane (here assumed to be the (x, z) one), respectively.

For the thermal simulations of the fiber, the external temperature was 25 °C, the silica thermal conductivity was 1.38 W/(m·K), the outer cladding thermal conductivity was 0.135 W/(m·K), and the convective heat transfer coefficient was 80 W/(m^2·K) at the outer physical boundary, which corresponds to a typical value for forced-air convection.

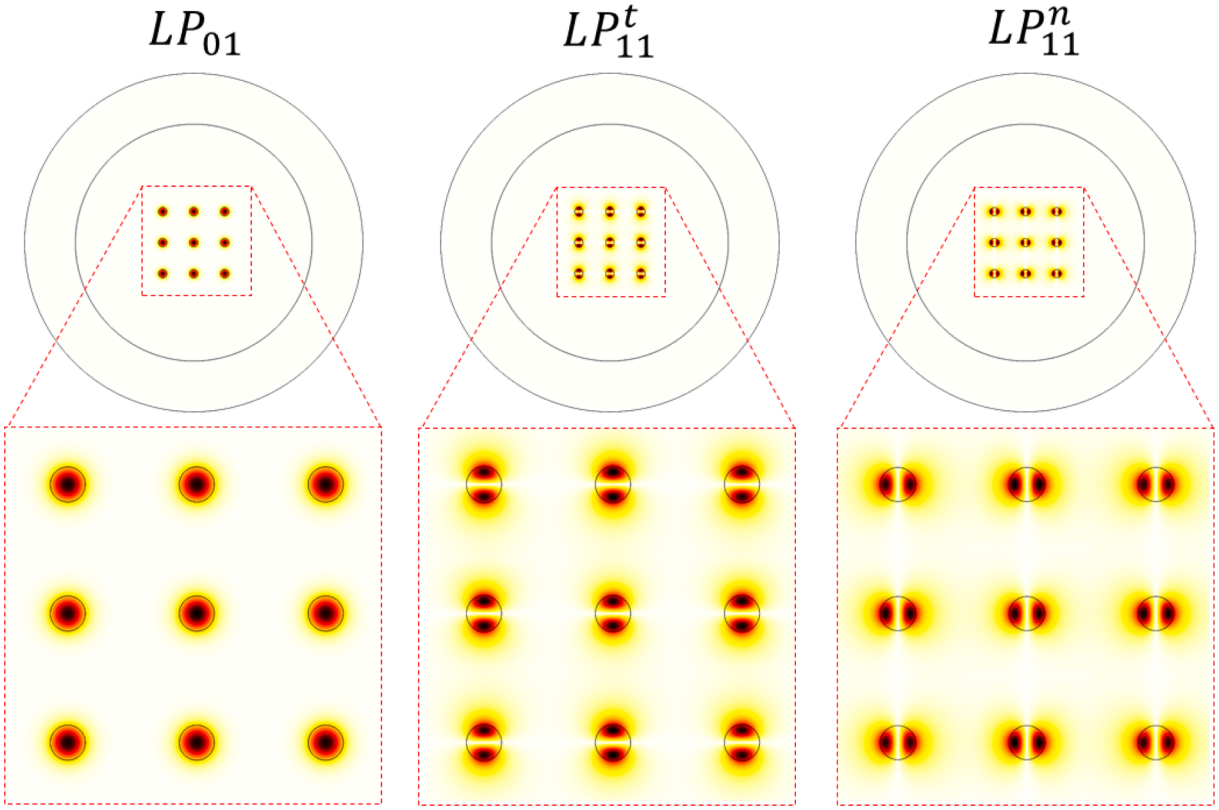

Fig. 2. Mode field distributions of a cold 9-core MCF with $\Lambda = 55$ μm and $d = 15$ μm.

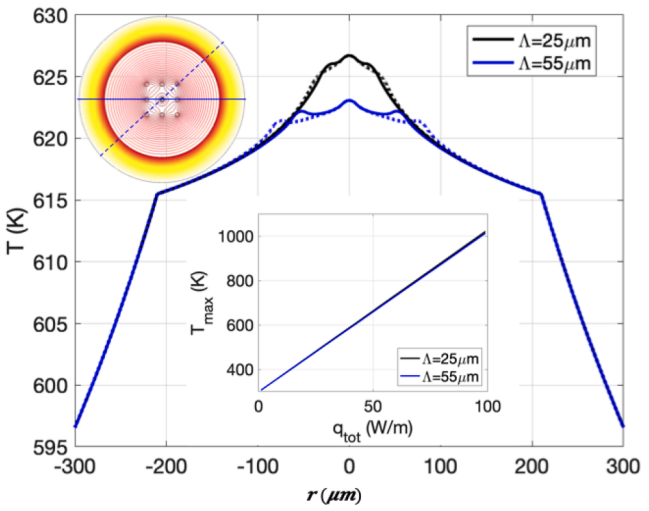

Fig. 3. Thermal profile across the 9-core multicore fiber for $d = 15$ μm and $q = 5$ W/m, along the x-axis (solid lines) and along the diagonal (dotted lines) for $\Lambda = 25$ μm (black) and $\Lambda = 55$ μm (blue). In the insets, isothermal contours for $q = 5$ W/m and $\Lambda = 55$ μm (top left), and peak temperature T_{max} at the fiber center versus the total heat load (center).

Fig. 3 shows the temperature profile for a heat load $q = 5$ W/m, for pitch values Λ of 25 μm and 55 μm. This results in a maximum temperature T_{max} in the center of the fiber cross-section, due to the combined heating effect of the neighboring cores, slightly increasing as the pitch is reduced and thus heat generation is concentrated. T_{max} increases linearly with the value of the total heat load q, as shown in the inset of Fig. 3, with a negligible dependence on the pitch. The analysis has been carried out by using the "COMSOL Multiphysics" commercial software package, which features specific numerical solvers aimed at various physics and engineering applications.

The effect of the thermal profile on the silica refractive index is taken into account through the thermo-optic effect model, where the material refractive index is modified by the thermally-induced index shift:

$$n(x,y,q) = n_0(x,y) + \beta[T(x,y,q) - T_0] \tag{1}$$

where $\beta = 1.16{\cdot}10^{-5}$ K^{-1} is the silica thermo-optic coefficient, $T(x,y,q)$ is the temperature profile calculated from the thermal simulation, and T_0 is the reference temperature at which the cold-fiber refractive index distribution $n_0(x,y)$ is given. The fiber refractive index is thus a function of both position and heat load q. From the temperature profile in Fig. 3 it can be observed that in the center core, where there is a concentration of the heat flux, the silica will undergo the greatest increase in the refractive index, and thus its FM will have the highest value of effective mode index, with respect to the side and corner core FMs effective indices. One of the main consequences of this is the breaking of the symmetry between cores, and thus the degeneration of the core FMs of the cold fiber is also broken.

The model takes into account the ideal cross-section of the fiber, without introducing geometrical imperfections or refractive index fluctuations as may be found in fabricated fibers. Such effects are either due to the tolerances inherent in the drawing process, or an index skew may be intentionally introduced between cores to reduce spurious coupling. The latter is done to exploit its property of impairing phase matching and thus core coupling. However, in the case of a model based on mode coupling, working on the ideal fiber actually corresponds to the worst case scenario of this particular problem.

The effects of fiber bending have been taken into account by using the conformal mapping technique, already successfully applied to take into account the bending effects in erbium doped fiber amplifiers [14]. By assuming to bend the fiber in the plane defined by the unit vectors $\hat{n}$ and $\hat{z}$, with $\hat{n}$ the unit vector normal to the bend direction and $\hat{z}$ the unit vector parallel to the fiber axis, the equivalent refractive index profile to be applied to the straight fiber geometry is given by

$$n_{eq}(x,y,q) = n(x,y,q)e^{\bar{r}\cdot\hat{n}/R_b} \tag{2}$$

where R_b is the bending radius, $\bar{r}$ the position vector, and $n(x,y,q)$ the fiber cross section refractive index modified by the temperature profile according to Eq. 1.

3. Optical coupling analysis

Optical decoupling between cores is key to optimal high-power MCF operation. We employ coupled mode theory analysis derived from two-core directional couplers [15]. We perform this analysis considering the absolute values of quantities like pitch and core diameter, considering value ranges for each quantity compatible with the limits (for example, on NA) given by the current technological processes.

Core-to-core coupling is evaluated in the case where one core is excited at a time, by calculating the maximum coupled power fraction (MCPF) between two modes indicated as i and j over a practical length L (1 m for rod MCFs and 10 m for coiled MCFs) as

$$P_{i,j} = max\{P_{i,j}(z)\} \quad for \quad 0 \leqslant z \leqslant L \tag{3}$$

where

$$P_{i,j}\left(z\right) = 4\left(\frac{|k_{i,j}|}{S_{i,j}}\right)^2 \sin^2\frac{S_{i,j}z}{2} \tag{4}$$

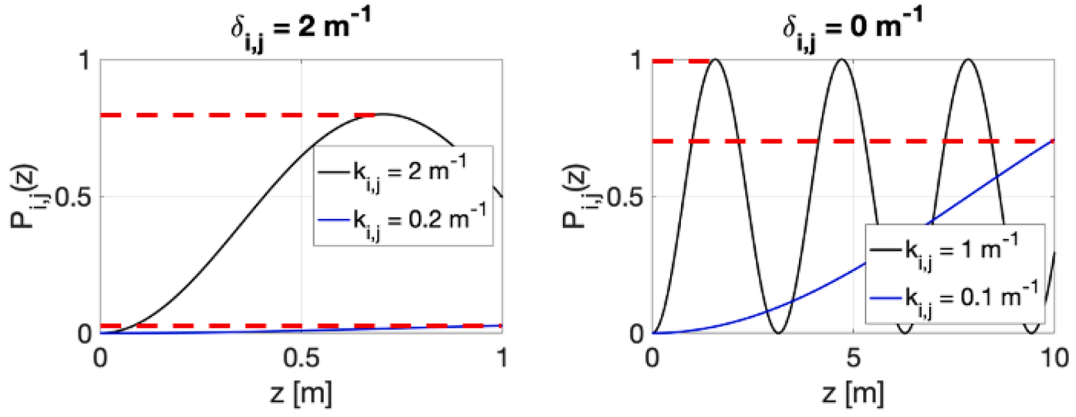

Fig. 4. Normalized coupled power evolution vs. fiber length for (left) mismatch coefficient $\delta_{i,j} = 2$ m^{-1} and $L = 1$ m length, and (right) no mismatch and $L = 10$ m length. The dashed red lines indicate the maximum coupled power fraction over length L for different values of $k_{i,j}$.

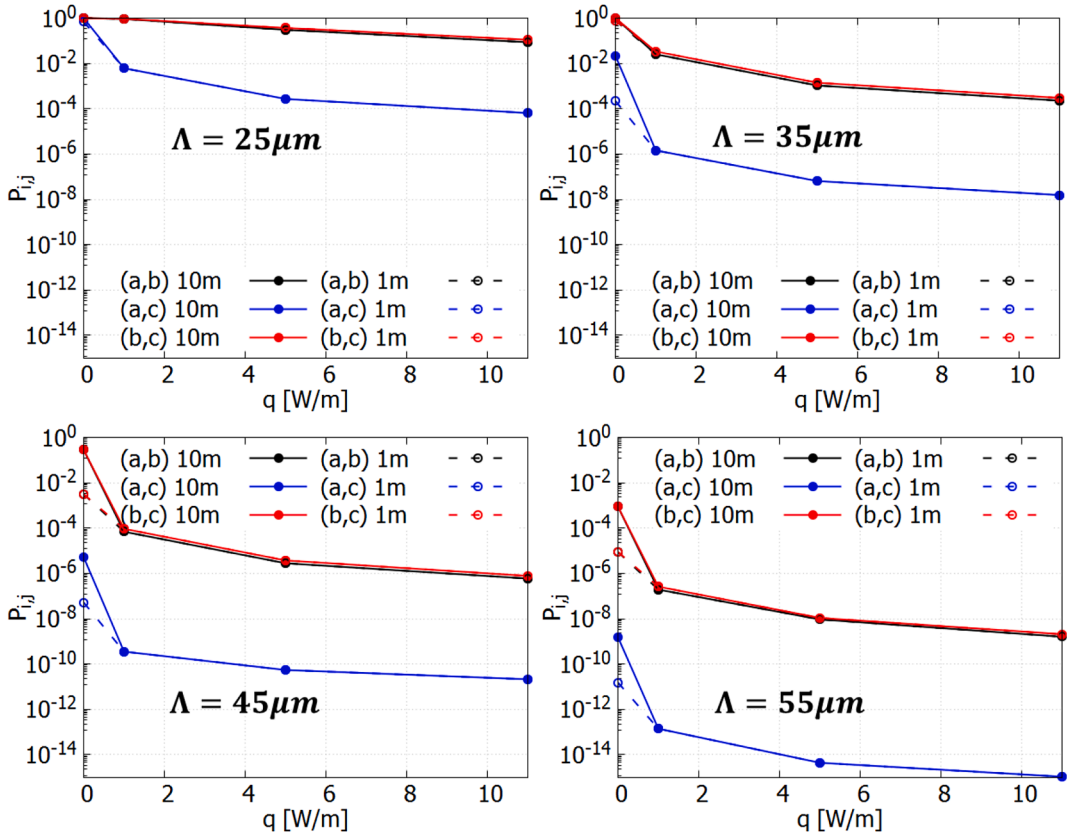

Fig. 5. Maximum power fraction coupled between FMs in different core families, in the first 1 m (dashed lines) and 10 m (solid lines) of propagation, for core diameter $d = 15$ μm and pitch Λ between 25 and 55 μm.

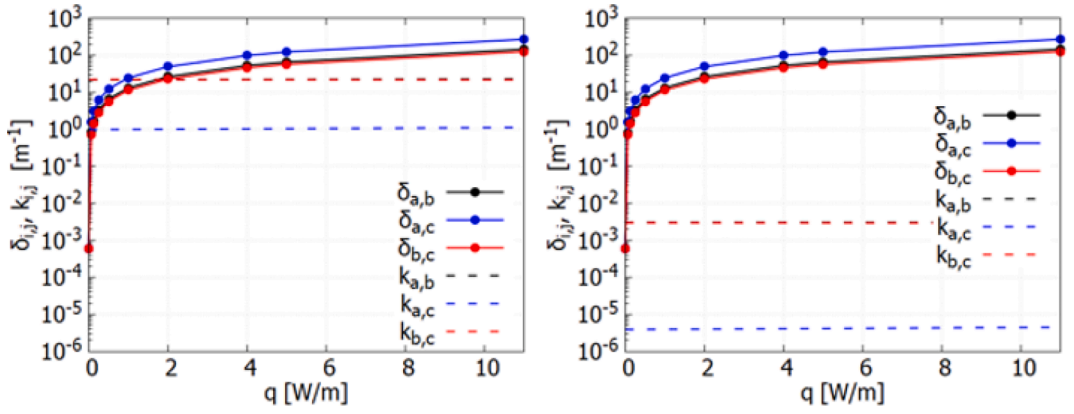

Fig. 6. Mismatch coefficient $\delta_{i,j}$ (solid lines) and coupling coefficient $k_{i,j}$ (dashed lines) for core diameter $d = 15$ μm and pitch $\Lambda = 25$ μm and 55 μm.

is the normalized coupled power as a function of fiber length, with

$$S_{i,j} = 2\sqrt{|k_{i,j}|^2 + \left(\frac{\delta_{i,j}}{2}\right)^2}. \tag{5}$$

This is defined as a function of the mismatch coefficient

$$\delta_{i,j} = \frac{2\pi\Delta n_{eff,ij}}{\lambda} \tag{6}$$

and of the coupling coefficient

$$k_{i,j} = \frac{\pi}{\lambda}\frac{1}{2\eta_0}\frac{\iint_{S_{d,i}}\left(n_{co,i}^2 - n_{cl}^2\right)\overline{E}_{t,i}\cdot\overline{E}_{t,j}dS}{\sqrt{P_i P_j}}. \tag{7}$$

In the previous formulas, $\Delta n_{eff,ij}$ is the effective index difference between modes i and j, η_0 is the intrinsic impedance of free space, $S_{d,i}$ is the active doped area of core i, S is the total fiber area, $\overline{E}_{t,i}$ and $\overline{E}_{t,j}$ are the transverse E-field components of modes i and j, and P_i, P_j are the total powers of modes i and j, respectively. For nonzero heating and bending, $n_{co,i}$ and n_{cl} become functions of heat load q and position (x, y) according to Eqs. 1 and 2. Also, $\overline{E}_{t,i}$ and $\overline{E}_{t,j}$ can be affected by thermal lensing and squeezing due to bending, and so they are functions of q and bending radius R_b.

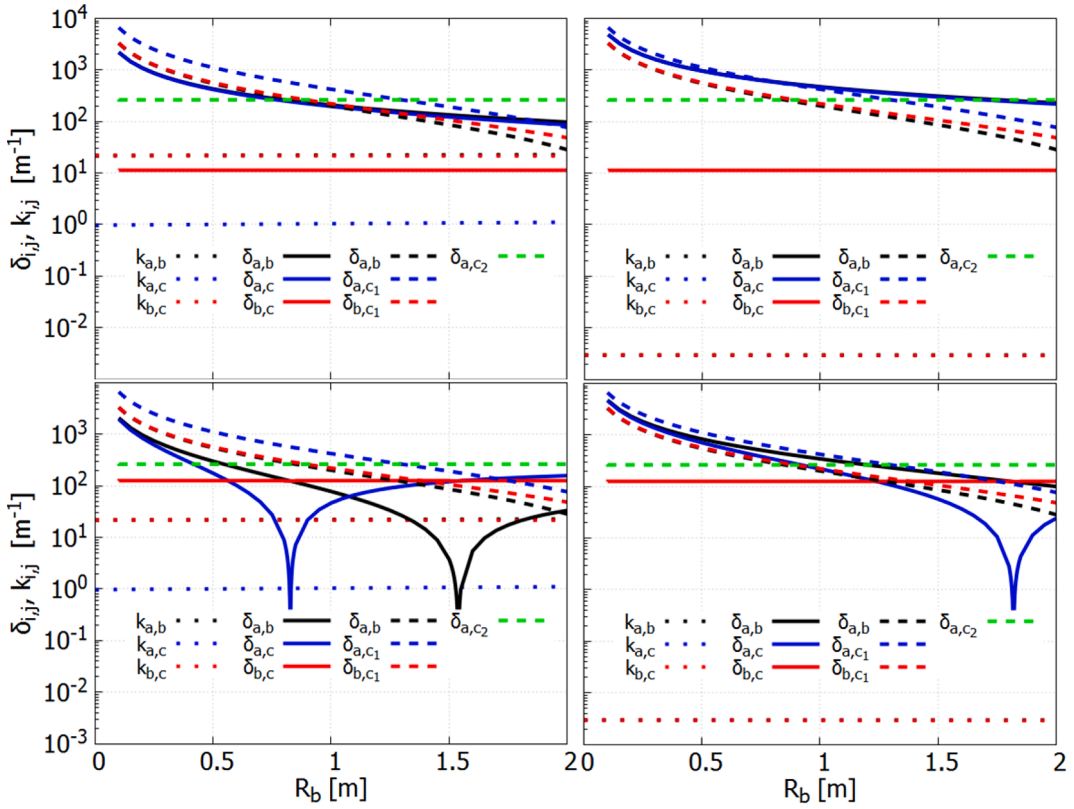

Fig. 7. Coupling coefficient $k_{i,j}$ (dotted lines) and mismatch coefficient $\delta_{i,j}$ for x-axis bending ($\hat{n} = \hat{x}$, solid lines) and diagonal bending ($\hat{n} = 1/\sqrt{2}(\hat{x} - \hat{y})$, dashed lines), for core diameter $d = 15$ μm, pitch $\Lambda = 25$ μm and 55 μm (left and right columns), and heat load $q = 1$ W/m and $q = 11$ W/m (top and bottom rows) for different values of the bending radius R_b.

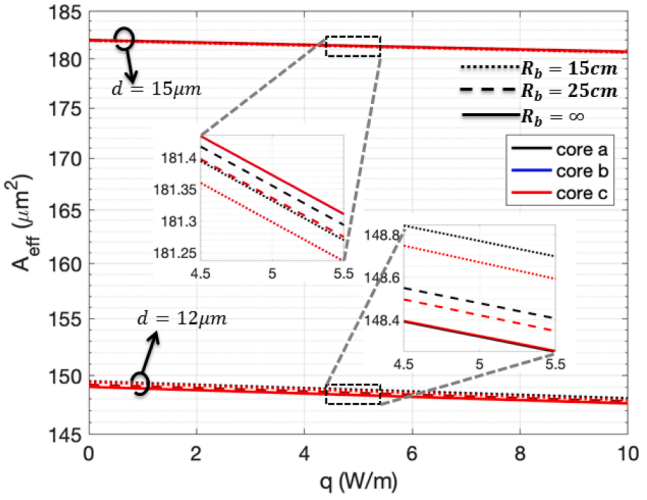

Fig. 8. Effective area of a single core in the 9-core MCF as a function of heat load q, for core diameter $d = 12$ μm (lower curves) and $d = 15$ μm (upper curves), and pitch $\Lambda = 35$ μm. The curves are given for the straight fiber (solid lines) and for the bent fiber with bending radius $R_b = 25$ cm (dashed lines) and $R_b = 15$ cm (dotted lines).

The relationship between coupling coefficient $k_{i,j}$, mismatch coefficient $\delta_{i,j}$, and fiber length L is shown in Fig. 4. A nonzero value of $\delta_{i,j}$ limits the maximum power transfer between modes i and j below unity, however the figure shows that this can only be reached if $k_{i,j}$ is high enough that such maximum is reached within the length of the fiber. Otherwise, power transfer will be limited to the value reached at the end of the fiber, which can be significantly lower than the maximum.

Geometrical and heat flow symmetries identify three different straight-fiber core families (a, b, and c) shown in Fig. 1, having a set radial distance from center. Fig. 5 shows the MCPF between FMs in different core families versus the heat load q for different pitches. For pitch of 45 μm or less, we have cold-fiber coupling, but a 1 W/m heat load is enough to cause uncoupling (i.e. a power fraction transferred within 10 m of 1% or less) down to 35 μm pitch. There was no difference between 1 m and 10 m lengths except for cold fiber, where coupling is minimal.

For better understanding of the reasons for the MCPF variations, we compare the mismatch coefficients with the coupling coefficients for 25 μm and 55 μm pitch, and heat loads from 0 to 11 W/m. Results are shown in Fig. 6. The phase mismatch increases with q, with slope dependent on core-to-core distance because of the temperature profile and independent of pitch. On the contrary, the $k_{i,j}$ show a negligible dependence on heat load and, as expected, a stronger dependence on pitch. So, the MCPF dependence on heat load is only due to $\delta_{i,j}$. Its value is negligible if either $k_{i,j} \ll \delta_{i,j}$ or $k_{i,j} \ll \pi/L$. For the lowest $\Lambda = 25$ μm, $k_{b,c}$ is not negligible with respect to either $\delta_{i,j}$ or π/L, so the improvement related with the $\delta_{i,j}$ increment is marginal. In this case, a mismatch coefficient greater than 10^3 m^{-1} would be required. This condition can be quite easily obtained in real fibers due to fabrication tolerances, however, as will be shown in Section V, the single-mode condition defines a lower bound for Λ.

Similarly, according to Eq. 2 bending can impair phase matching, as shown in Fig. 7 where $\delta_{i,j}$ are plotted versus the bending radius R_b for two pitches (25 μm and 55 μm), heat loads (1 W/m and 11 W/m), and bending planes ($\hat{n} = \hat{x}$ and $\hat{n} = 1/\sqrt{2}(\hat{x} - \hat{y})$). The notches are due to phase matching when thermal and bending effects cancel out, however they occur at larger than practical radii, and not in straight (i.e. rod) fibers. For x-axis bending, $\delta_{b,c}$ is constant with R_b because of the same

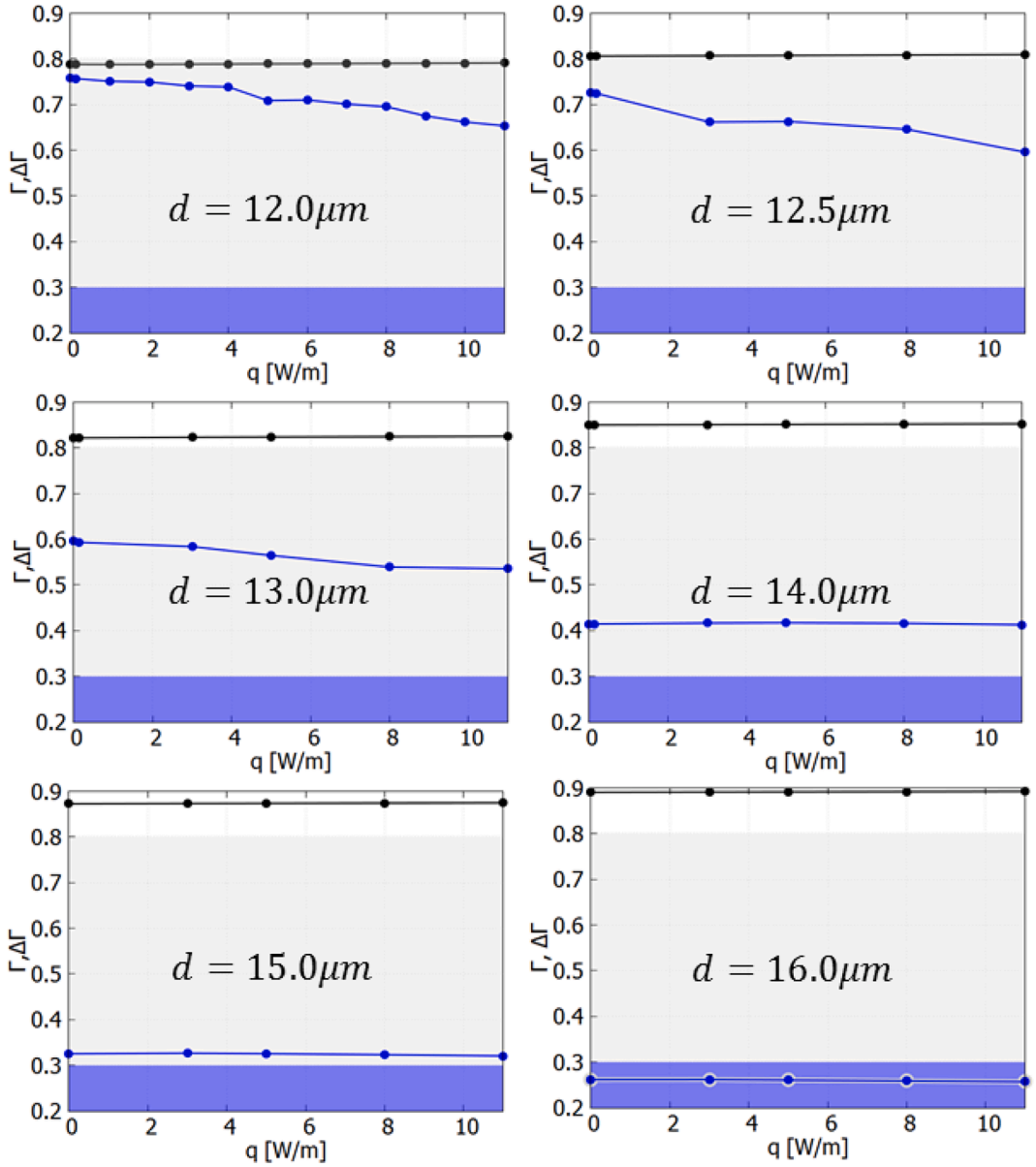

Fig. 9. Modal overlap Γ_{FM} (black curves) and overlap difference $\Delta\Gamma$ (blue curves), for a 9-core MCF with pitch $\Lambda = 55$ μm and core diameter d variable between 12 and 16 μm. The region where $\Gamma_{FM} > 0.8$ is depicted by the white area, while the region where $\Delta\Gamma < 0.3$ is depicted by the blue area.

index change on cores b and c. For diagonal bending, core pair (a, c_1) is not affected, though having higher mismatch than (b, c) due to higher distance. Dependence of $k_{i,j}$ on bending radius and plane is also very weak, therefore Fig. 7 reports just one set of curves; FM coupling is confirmed to be dominated by phase matching. In summary, there is always a core pair that cannot be improved by bending due to constant refractive index difference for varying R_b, and this sets the limit: the worst case is the (b, c) pair for x-axis bending.

4. Effective area

In high power applications, the effective area A_{eff} is an important figure of merit, since it permits to reduce fiber damage and nonlinear effects. In LMAFs, A_{eff} is strongly affected by thermal effects due to thermal lensing, and also by bending, which causes the guided field to be squeezed towards the outside of the bent fiber [16].

In order to analyze thermal and bending effects in MCFs, we calculated the FM effective area of each core i as

$$A_{eff,i} = \frac{\left(\iint_S |\overline{E_i}|^2 dS\right)^2}{\iint_S |\overline{E_i}|^4 dS} \tag{8}$$

for different core diameters, heat loads, and bending radii. Due to the envisioned lack of core coupling, we performed three single-core simulations (a, b, and c) to calculate the total effective area A_{eff}. We compared the straight fiber case with the bent fiber for bending radii of 15 and 25 cm, as a function of heat load q. We considered the fibers with core diameters $d = 12$ μm ($A_{eff} = 148$ μm^2) and $d = 15$ μm ($A_{eff} = 181$ μm^2).

As shown in Fig. 8, the effective area only slightly decreases for increasing heat load from 0 to 10 W/m, by 0.9% for the 12 μm core fiber and by 0.6% for the 15 μm core one. Bending the fiber up to a radius $R_b = 15$ cm has an even smaller effect on the effective area, varying by 0.3% for the 12 μm core fiber and by 0.05% for the 15 μm core one, showing negligible FM squeezing. Core b and core c are almost

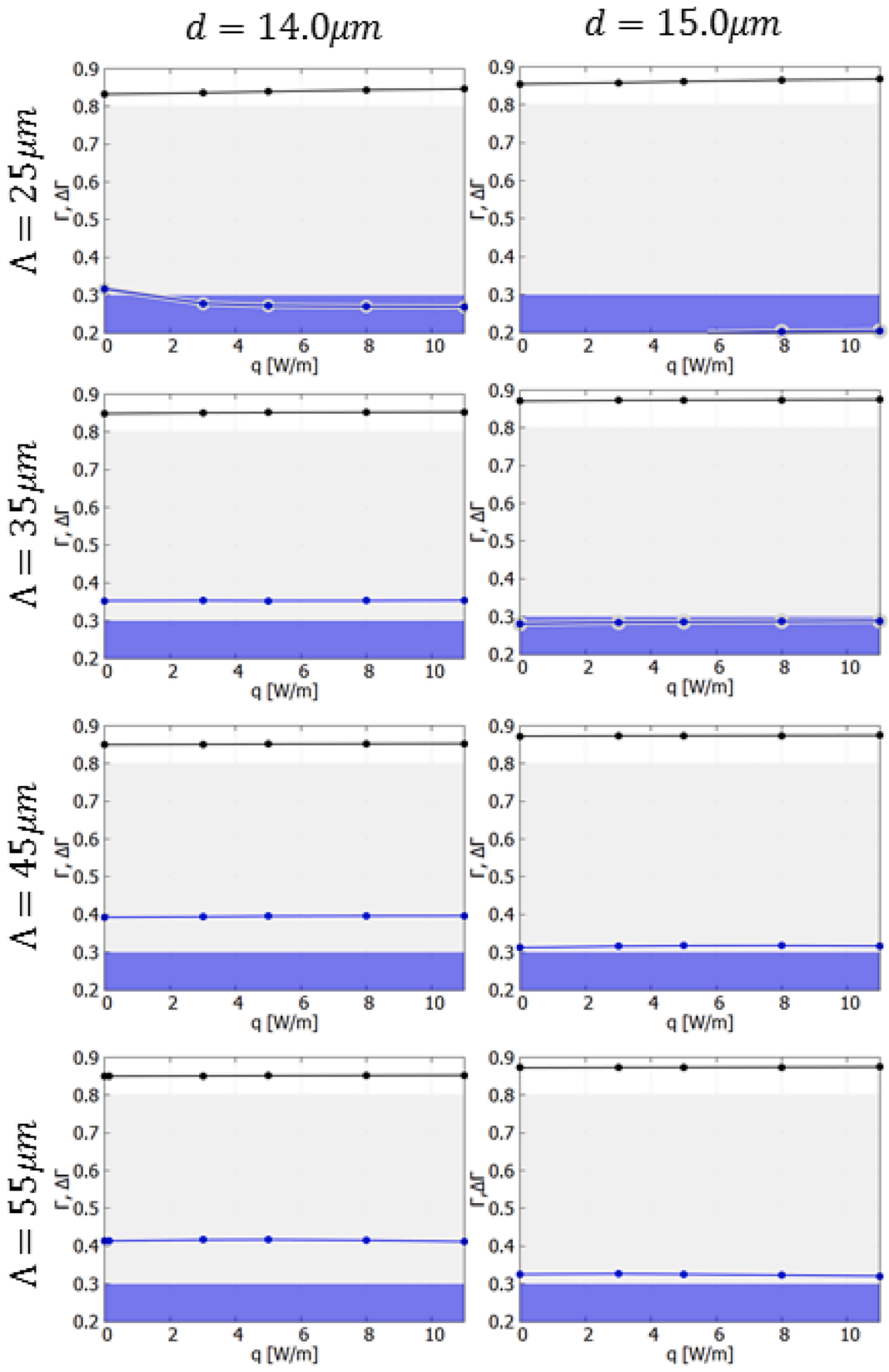

Fig. 10. Modal overlap Γ_{FM} (black curves) and overlap difference $\Delta\Gamma$ (blue curves), for a 9-core MCF with core diameter $d = 14$ μm (left column) and $d = 15$ μm (right column), and pitch Λ variable between 25 and 55 μm (from top to bottom). The region where $\Gamma_{FM} > 0.8$ is depicted by the white area, while the region where $\Delta\Gamma < 0.3$ is depicted by the blue area.

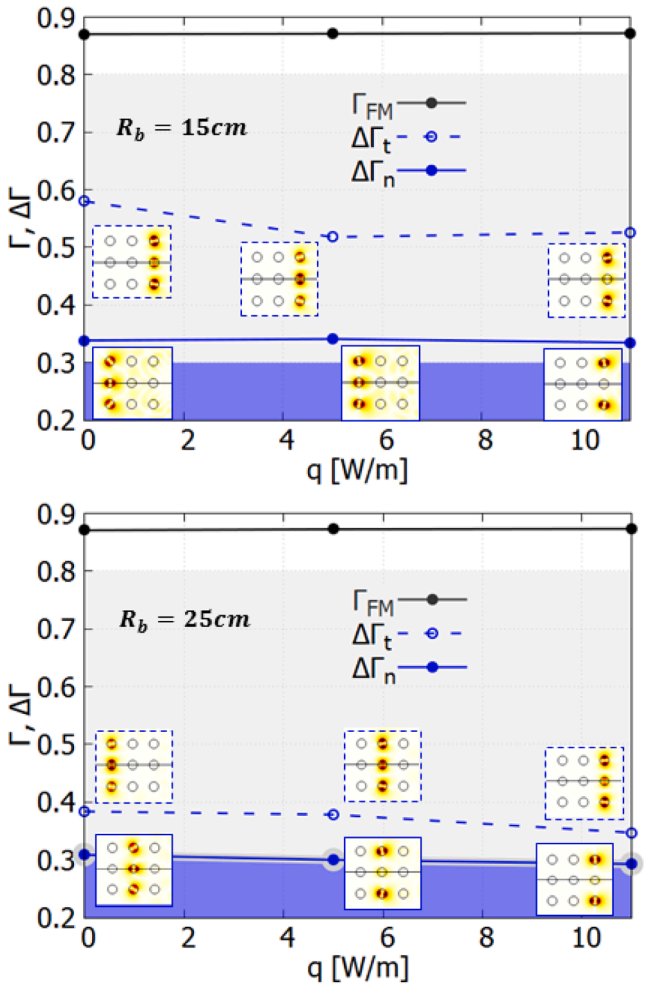

Fig. 11. Modal overlap Γ_{FM} (black curves) and minimum overlap difference $\Delta\Gamma$ (blue curves) of the HOMs LP^n_{11} (solid) and LP^t_{11} (dashed), for a 9-core MCF with core diameter $d = 15$ μm and pitch $\Lambda = 35$ μm, for bending radius R_b of 15 (top) and 25 cm (bottom). Insets show the LP^n_{11} and LP^t_{11} modes with the lowest $\Delta\Gamma$. The region where $\Gamma_{FM} > 0.8$ is depicted by the white area, while the region where $\Delta\Gamma < 0.3$ is depicted by the blue area.

indistinguishable from each other with respect to this behaviour. The effective area dependence from temperature and bending is higher for lower core diameter as in that case the V-number is reduced, giving lower confinement and higher sensitivity to such effects. The different trend of A_{eff} for $d = 12$ μm and $d = 15$ μm means that in the first case the effect of lower confinement prevails, whereas in the latter the mode squeezing due to bending does.

However, such variations are very small anyway, and confirm the high stability of the electric field distribution for varying heat load and bending. Though a direct comparison between a multi-core and a single-core fiber is not straightforward, in the context of a multi-beam combining scheme, a fair assessment can be given by considering a single-core fiber with an area $A_{eq} = \sqrt{N}\cdot A$, where A is the area of a single core and N is the number of cores in the multi-core fiber [17]. In this case, the area of the single-core fiber is effectively tripled, which increases the sensitivity of the fiber to bending and thermal lensing.

5. Effectively single-mode condition

After considering the effects of mode coupling in itself, and the effective area sensitivity, we estimated the effect of thermally-induced coupling on the amplification process, by considering criteria based on the effective monomodality of the cores. In this respect, standard LMA

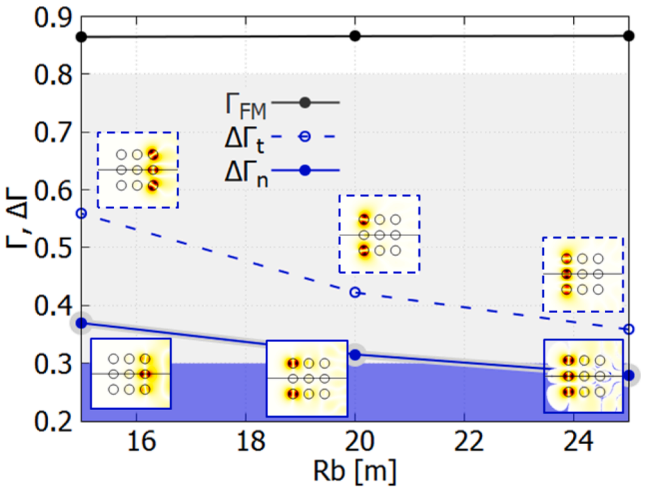

Fig. 12. Modal overlap Γ_{FM} (black curves) and minimum overlap difference $\Delta\Gamma$ (blue curves) of the HOMs LP^n_{11} (solid) and LP^t_{11} (dashed), for a 9-core MCF with core diameter $d = 15$ μm and pitch $\Lambda = 25$ μm, for heat load $q = 5$ W/m and bending radius R_b ranging from 15 to 25 cm. Insets show the LP^n_{11} and LP^t_{11} modes with the lowest $\Delta\Gamma$. The region where $\Gamma_{FM} > 0.8$ is depicted by the white area, while the region where $\Delta\Gamma < 0.3$ is depicted by the blue area.

fibers suffer from changes in the electric field distribution caused by heat load, in particular by thermal lensing, which makes the fiber no longer single-mode.

To this end, we modelled how the heat load affects the overlap integral Γ of the guided modes defined as

$$\Gamma_{k,i} = \iint_{S_{d,i}} i_k\left(x,y\right) dx\,dy \tag{9}$$

where $S_{d,i}$ is the active doped area of core i and $i_k(x,y)$ is the normalized field intensity $i_k(x,y) = Re(p_{z,k}/P_k)$ of a certain mode k, where P_k is the total power of the mode and $p_{z,k}$ is the magnitude of the longitudinal component of the Poynting vector, which is defined as

$$\overline{p}_k = \frac{1}{2}\overline{E}_k \times \overline{H}_k^* \tag{10}$$

where $\overline{E}_k$ and $\overline{H}_k$ are the electric and magnetic field vectors of the mode, respectively. Γ gives a measure of the fraction of modal intensity which is confined inside the core and thus of the modal gain per unit length. The overlap integral difference $\Delta\Gamma = \Gamma_{FM} - \Gamma_{HOM}$ between FM and the HOM with the greatest overlap gives account of the different FM and HOMs amplification gain. According to an empirical criterion which has been proposed and widely accepted to define the operation of the amplifier as effectively single-mode, it is required for Γ_{FM} to remain above 0.8, while $\Delta\Gamma$ should be greater than 0.3 [18,19], so that the FM will absorb enough of the gain reservoir and at the same time the HOMs will be delocalized enough from the core to prevent the HOMs themselves from being effectively amplified. In a multicore fiber, effective monomodality is limited by the core that has the worst overlap integral difference in each of the analyzed conditions, and thus it is the one which is intended in the following.

To give a detailed account of this phenomenon, the influence of two key design parameters as core diameter and pitch on $\Delta\Gamma$ when different q values are simultaneously applied to all cores was thoroughly investigated as shown in Figs. 9 and 10. Finding the optimal combination of pitch and core diameter to ensure single-mode operation is one of the crucial steps required to set a clear direction to improve the fiber performance.

Fig. 9 considers the evolution of the effectively single-mode

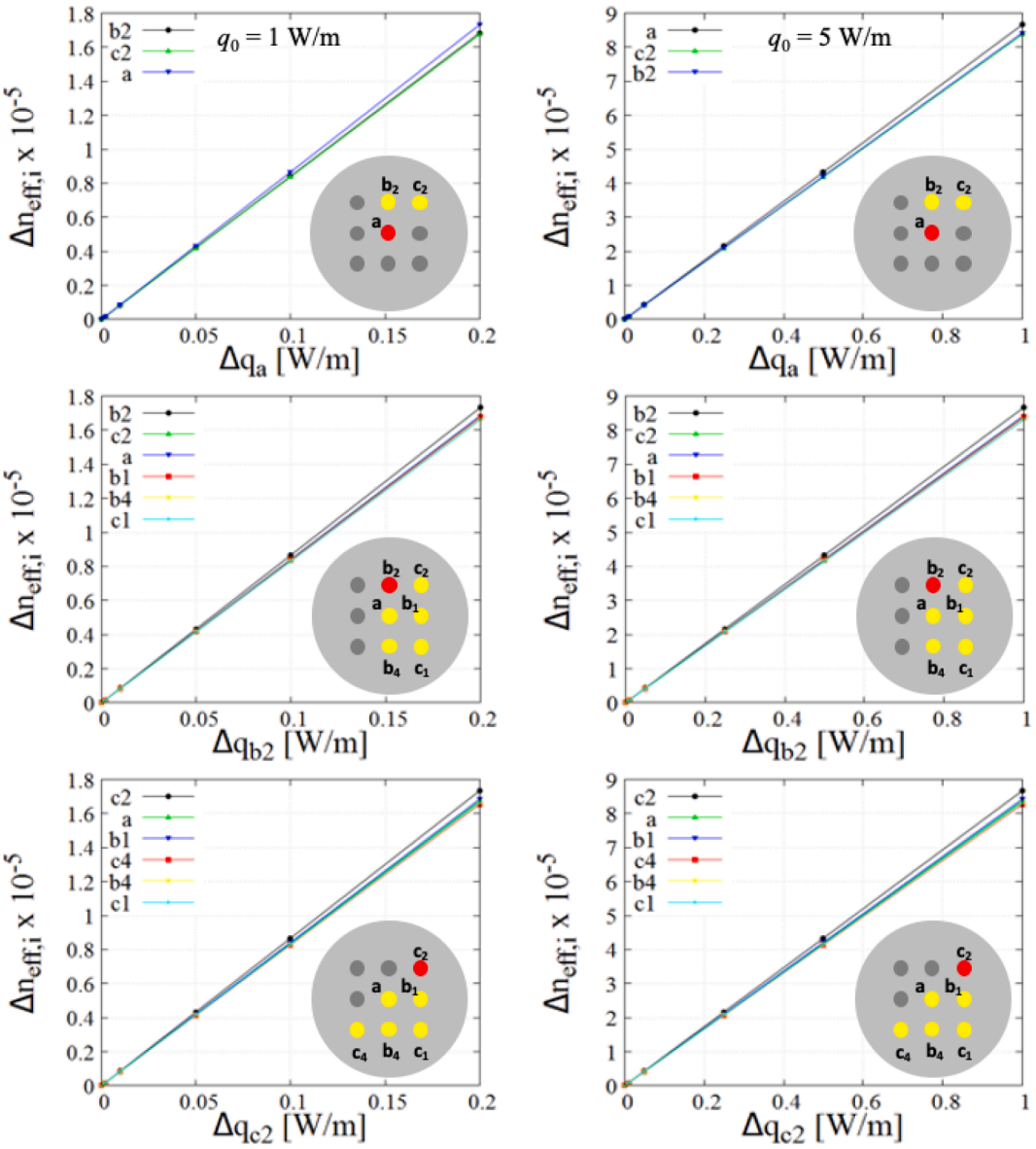

Fig. 13. Effective index variation Δn_{eff} of FM as a function of heat load variation Δq_i applied to core a (top row), b_2 (middle row), and c_2 (bottom row) at $q_0 = 1$ W/m (left column) and $q_0 = 5$ W/m (right column), for the cores indicated in the inset in each row. The inset shows the core where the heat load variation is applied in red and the cores where the effective index variation is estimated in yellow.

condition for large pitch $\Lambda = 55$ μm, where the FM overlap is little influenced by heat load, while up to $d = 13$ μm (where the single core's V-number is within the monomodality range), Γ_{HOM} is increasing with q due to HOMs having low guidance in the cold fiber, which increases with heat load. For $d > 13$ μm (where the single core's V-number is in the multimode range), Γ_{FM} and $\Delta\Gamma$ are essentially independent of heat load, as the modes' confinement in the core saturates. According to the aforementioned criteria, the fiber remains effectively single-mode up to $d = 15$ μm, which sets the absolute effective area limit. Taking this core diameter as reference and studying the performance for varying pitch in Fig. 10, it can be seen that the pitch can be reduced down to $\Lambda = 35$ μm before losing effective monomodality. It is verified that, for this core diameter value, a high heat load does not impair the effectively single-mode condition.

Reducing the core diameter in order to trade off lower effective area with greater compactness due to lower pitch is only partially possible. In fact, by repeating the same study with reduced core diameter $d = 14$ μm in Fig. 10, it can be seen that the effectively single-mode condition still holds down to $\Lambda = 35$ μm. In straight fibers, $\Lambda \simeq 35$ μm appears as a lower bound in terms of both optical coupling and effective monomodality. By bending the fiber, the effective monomodality lower bound can be further reduced. Fig. 11 shows the Γ_{FM} and $\Delta\Gamma$ for different pitches, heat loads and bending radii. The HOMs with the highest overlap integral are LP^n_{11} and LP^t_{11}, identified by having the zero intensity line normal and tangential to the bending plane, respectively. Once more, the insensitivity of the FM E-field guarantees the stability of Γ_{FM} and thus of the amplification process. Conversely, a dependence of the HOMs on R_b is observed. By reducing R_b, their overlaps reduce, improving the $\Delta\Gamma$ values. This dependence is different for HOMs LP^n_{11} and LP^t_{11}. Their intensity distributions are shown in the inboxes of Fig. 11 and, due to the orientation of the LP^n_{11} and LP^t_{11} mode field distributions varying continuously from a pure mode to an increasingly slanted one with increasing bending, we labeled the bent distributions according to the corresponding ones without bending. The worst case is always given by LP^n_{11}, which are more localized than LP^t_{11} modes. Results in Fig. 12 show that bending can help to reach the effectively single-mode condition also for pitches lower than 35 μm without affecting Γ_{FM}.

6. Thermal coupling analysis

For the optimum fiber parameters of $d = 15$ μm and $\Lambda = 35$ μm found in the previous section, we evaluated the effect of the heat load variation around a set point in only one of the cores on the effective index of the FM in all cores. The heat load variation in a single core can cause thermal coupling between cores [8]. For symmetry reasons, it is only necessary to consider heat load applied to cores a, b_2, and c_2, and the effects need to be evaluated only in some of the cores, as depicted in the insets of Fig. 13.

We considered for the set point the values of $q_0 = 1$ W/m and 5 W/m, and the considered variation Δq_i was up to 20%. The results shown in Fig. 13 reveal that for these geometrical parameters, the long-range effective index difference caused by heating variations in a distant core is not enough to give significant disparities of effect in the phasing of the different cores: the corresponding effective index variation Δn_{eff} is up to 4.7% for the FM in the worst case (heating of core c_2), and this value remains the same even at the greater proportional heat load swing obtained at $q_0 = 1$ W/m.

7. Conclusion

In this work, thermal and bending effects on MCFs for high power lasers and amplifiers have been numerically investigated in terms of optical and thermal coupling, effective area, and effectively single-mode behaviour.

MCFs proved to be very robust to the stressing factors here considered. Their properties are little affected by heat load and bending radius. The parameters related to the effective index, such as the coupling coefficient, are a little bit more sensitive to the applied changes than the ones associated to the field distribution, such as the core overlap integral and the effective area.

However, they even allow to improve the fiber performance. The thermal profile caused by heat load breaks the natural degeneracy of the FMs in the cores, which are assumed to be all identical, reducing the coupling of the optical cores and allowing a smaller pitch and a higher number of cores per unit area within the cross-section. Bending does not have significant effects on coupling and effective area, while it reduces HOM core overlap, to the benefit of effective monomodality.

The increase of the core diameter guarantees a larger effective mode area, but at the same time it causes a reduction of the overlap difference between FM and HOM, which puts an upper bound on the core diameter, and thus on the achievable modal effective area. Also, pitch reduction tends to slightly decrease that upper bound.

Numerical results show that effectively single-mode behaviour can be obtained with core diameters of 15 μm, corresponding to an effective area of 181 μm^2 per core, with a pitch of 35 μm for straight and bent fibers, with a total core occupied area of 85×85 μm^2.

The presented analysis gives useful guidelines for design and optimization of MCFs for high power lasers and amplifiers. The results and the guidelines can be easily extended to MCFs with a greater number of cores, such as 4×4 cores or more.

CRediT authorship contribution statement

Lorenzo Rosa: Conceptualization, Investigation, Methodology, Software, Supervision, Validation, Visualization, Writing – original draft, Writing – review & editing. **Seyyedhossein Mckee:** Investigation, Software, Validation, Visualization, Writing – original draft, Writing – review & editing. **Federica Poli:** Conceptualization, Investigation, Writing – original draft. **Annamaria Cucinotta:** Conceptualization, Investigation, Methodology, Resources, Supervision, Writing – original draft. **Luca Vincetti:** Conceptualization, Investigation, Methodology, Resources, Supervision, Validation, Visualization, Writing – original draft, Writing – review & editing.

Declaration of Competing Interest

The authors declare that they have no known competing financial interests or personal relationships that could have appeared to influence the work reported in this paper.

References

[1] J.W. Dawson, M.J. Messerly, R.J. Beach, M.Y. Shverdin, E.A. Stappaerts, A. K. Sridharan, P.H. Pax, J.E. Heebner, C.W. Siders, C. Barty, Analysis of the scalability of diffraction-limited fiber lasers and amplifiers to high average power, Opt. Express 16 (17) (2008) 13240–13266, https://doi.org/10.1364/OE.16.013240.

[2] A. Tünnermann, T. Schreiber, F. Röser, A. Liem, S. Höfer, H. Zellmer, S. Nolte, J. Limpert, The renaissance and bright future of fibre lasers, J. Phys. B 38 (9) (2005) S681–S693, https://doi.org/10.1088/0953-4075/38/9/016.

[3] C. Jauregui, J. Limpert, A. Tünnermann, High-power fibre lasers, Nat. Photonics 7 (11) (2013) 861–867, https://doi.org/10.1038/nphoton.2013.273.

[4] T. Eidam, C. Wirth, C. Jauregui, F. Stutzki, F. Jansen, H.-J. Otto, O. Schmidt, T. Schreiber, J. Limpert, A. Tünnermann, Experimental observations of the threshold-like onset of mode instabilities in high power fiber amplifiers, Opt. Express 19 (14) (2011) 13218–13224, https://doi.org/10.1364/OE.19.013218.

[5] H.J. Otto, A. Klenke, C. Jauregui, F. Stutzki, J. Limpert, A. Tünnermann, Scaling the mode instability threshold with multicore fibers, Opt. Lett. 39 (9) (2014) 2680–2683, https://doi.org/10.1364/OL.39.002680.

[6] J. Limpert, Ultra-large mode area fibers for high power lasers, in: Advanced Photonics 2018, Optical Society of America, 2018, p. SoM4H.2. doi:10.1364/SOF.2018.SoM4H.2.

[7] J. Lægsgaard, F. Poli, A. Cucinotta, S. Selleri, Theory of thermo-optic instabilities in dual-core fiber amplifiers, Opt. Lett. 43 (19) (2018) 4775–4778, https://doi.org/10.1364/OL.43.004775.

[8] L. Rosa, S.H. Pallangal, F. Poli, S. Selleri, A. Cucinotta, Mode phase variation and sensitivity to thermal load in three-core optical fibers, J. Lightwave Technol. 38 (8) (2020) 2400–2405, https://doi.org/10.1109/JLT.2020.2964636.

[9] A. Steinkopff, C. Jauregui, C. Aleshire, A. Klenke, J. Limpert, Impact of thermo-optical effects in coherently combined multicore fiber amplifiers, Opt. Express 28 (25) (2020) 38093–38105, https://doi.org/10.1364/OE.410614.

[10] C. Jollivet, A. Mafi, D. Flamm, M. Duparré, K. Schuster, S. Grimm, A. Schülzgen, Mode-resolved gain analysis and lasing in multi-supermode multi-core fiber laser, Opt. Express 22 (24) (2014) 30377–30386, https://doi.org/10.1364/OE.22.030377.

[11] L. Rosa, S. Mckee, L. Vincetti, F. Poli, S. Selleri, A. Cucinotta, Thermo-optic effects in multicore fibers for high-power lasers, in: M. Ferrari, J.I. Mackenzie, S. Taccheo (Eds.), Fiber Lasers and Glass Photonics: Materials through Applications II, vol. 11357, International Society for Optics and Photonics, SPIE, 2020, pp. 165–170, https://doi.org/10.1117/12.2563934.

[12] L. Rosa, E. Coscelli, F. Poli, A. Cucinotta, S. Selleri, Thermal modeling of gain competition in Yb-doped large-mode-area photonic-crystal fiber amplifier, Opt. Express 23 (14) (2015) 18638–18644, https://doi.org/10.1364/OE.23.018638.

[13] E. Coscelli, R. Dauliat, F. Poli, D. Darwich, A. Cucinotta, S. Selleri, K. Schuster, A. Benoit, R. Jamier, P. Roy, F. Salin, Analysis of the Modal Content Into Large-Mode-Area Photonic Crystal Fibers Under Heat Load, IEEE J. Sel. Top. Quantum Electron. 22 (2) (2016) 323–330, https://doi.org/10.1109/JSTQE.2015.2479156.

[14] L. Vincetti, M. Foroni, F. Poli, M. Maini, A. Cucinotta, S. Selleri, M. Zoboli, Numerical Modeling of S-Band EDFA Based on Distributed Fiber Loss, J. Lightwave Technol. 26 (14) (2008) 2168–2174, https://doi.org/10.1109/JLT.2008.923221.

[15] S. Selleri, L. Vincetti, A. Cucinotta, Optical and Photonic Components, second ed., Esculapio, Bologna, Italy, 2015.

[16] L. Dong, Thermal lensing in optical fibers, Opt. Express 24 (17) (2016) 19841–19852, https://doi.org/10.1364/OE.24.019841.

[17] C. Jauregui, J. Limpert, A. Tünnermann, Ultra-large mode area fibers for high power lasers, in: Optical Fiber Communication Conference, Optical Society of America, 2018, p. M2J.1. doi:10.1364/OFC.2018.M2J.1.

[18] M.M. Jørgensen, S.R. Petersen, M. Laurila, J. Lægsgaard, T.T. Alkeskjold, Optimizing single mode robustness of the distributed modal filtering rod fiber amplifier, Opt. Express 20 (7) (2012) 7263–7273, https://doi.org/10.1364/OE.20.007263.

[19] J.-P. Yehouessi, O. Vanvincq, A. Cassez, M. Douay, Y. Quiquempois, G. Bouwmans, L. Bigot, Extreme large mode area in single-mode pixelated bragg fiber, Opt. Express 24 (5) (2016) 4761–4770, https://doi.org/10.1364/OE.24.004761.